The Hidden Effects of Particle Shape and Criteria for Evaluating the Upconversion Luminescence of the Lanthanide Doped Nanophosphors

ARTICLE *in* THE JOURNAL OF PHYSICAL CHEMISTRY C · FEBRUARY 2010

Impact Factor: 4.77 · DOI: 10.1021/jp908976n

5 AUTHORS, INCLUDING:

Mruthunjaya Uddi
Massachusetts Institute of Technology
39 PUBLICATIONS **598** CITATIONS

SEE PROFILE

Nan Yao
Princeton University
158 PUBLICATIONS **5,243** CITATIONS

SEE PROFILE

The Hidden Effects of Particle Shape and Criteria for Evaluating the Upconversion Luminescence of the Lanthanide Doped Nanophosphors

Jingning Shan,*,† Mruthunjaya Uddi,† Robert Wei,† Nan Yao,‡ and Yiguang Ju†

Department of Mechanical and Aerospace Engineering, Princeton University, Princeton, New Jersey 08544, and Princeton Institute for the Science and Technology of Materials, Princeton University, Princeton, New Jersey 08544

Received: September 16, 2009; Revised Manuscript Received: December 22, 2009

The dependences of upconversion luminescence (UCL) on the particle size, shape, and inorganic−ligand interface of the hexagonal (β)-phase $NaYF_4$:Yb,Er upconversion nanophosphors (β-UCNPs) were studied. The photophysical data, e.g., relative UCL intensity, power-dependent UCL, green to red emission intensity ratio ($f_{g/r}$), and dynamic luminescence lifetimes of the prism-, plate-, and rod-shaped β-UCNPs as a function of surface to volume (SA/Vol) ratio were investigated. It was found that the UC properties can be attributed to not only the surface effects by comparing the SA/Vol ratios but also the particle shapes. At the comparable SA/Vol and ion (Yb/Er) doping ratios (20%/2%), the prism-shaped UCNPs showed much larger UCL intensity and smaller saturation power than those of the rod-shaped UCNPs. The shape effects on the UCL were also confirmed from the $f_{g/r}$ and photodynamic results on the fluorescence decay time. We attribute the shape effects to the different fractional lattice components in an anisotropic orientational β-nanocrystal in which the *a*-axis and *c*-axis have the crystal planes of $\langle 10\bar{1}0\rangle$ and $\langle 0001\rangle$ families, respectively, with different *d*-spacing distances. Therefore, the differently shaped nanocrystals with identical SA/Vol ratios could have different lattice energy and multiphonon relaxation processes. Aiming at clarifying the current contradictory observations on the UCL, three general criteria, namely, (i) a particle size window with a consistent shape, (ii) systematic investigation of $f_{g/r}$ as a function of the excitation power, and (iii) comparable UC hosts and surface properties, for assessing the UCL of the UCNPs are proposed. The observations reported here add an alternative point of view of understanding the energy transfer in the rare earth doped NPs, which should be useful for testing theories of optical confinement of the lanthanide-doped NPs and provide new strategies for both fundamental and technological interest like those well-known colloidal semiconductor quantum dots and rods.

I. Introduction

In recent years, interest in rare earth (Ln^{3+}, Ln = Er, Tm, and Ho) codoped with Yb^{3+} for near-infrared (NIR)-to-visible upconversion nanophosphors (UCNPs) has grown considerably due to their potential applications in diverse fields, e.g., for biolabeling,[1,2] photodynamic therapy (PDT),[3−5] security, and energy.[6,7] Selection of a suitable host for Yb,Ln ions is one of the key issues to preparing size and shape controllable UCNPs and to achieving efficient upconversion luminescence (UCL); so far, the most efficient UC host is the hexagonal (β)-phase $NaYF_4$.[8−10] Yan reported the first cothermolysis method to obtain oleate (OA) ligated β-phase $NaYF_4$:Yb,Ln UCNPs (abbreviated as β-UCNPs).[11] In subsequent work, significant achievements in the synthesis,[12−19] surface modifications,[4,17,19−21] and photophysical studies[22−24] of the hydrophobically ligated UCNPs were reported. However, the lack of a fundamental understanding of the nanoscale size and shape-dependent UCL still remains a great challenge.

The UC process in the β-UCNPs has been verified to be an energy transfer upconversion (ETU) involving the cross relaxation (radiative or nonradiative) at intermediate energy levels among Ln^{3+} and Yb^{3+} ions.[25] The Yb^{3+} ion acts as the sensitizer to collect and transfer two or more low energy photons (e.g., 980 nm) to the Ln^{3+} ions, and visible UCL at a higher energy is generated from excited states down to the ground state in Ln^{3+}. The decreasing UCL due to the reduction of the particle size has been observed.[13,15,26] Under the comparable conditions of the ensemble UCNPs, e.g., hosts, crystalline phases, dopant concentrations, and activator (Yb^{3+}) to acceptor (Ln^{3+}) ratios, the decreasing dependence of UCL on the particle sizes has been ascribed to the surface defects[22] and restricted phonon relaxation,[27] respectively. For surface defects, in general, the smaller UCNPs have larger surface to volume (SA/Vol) ratios and therefore more fractions of quenching defects than those of the larger UCNPs. These cause more nonradiative decay and diminished UCL intensity;[22] for restricted phonon relaxation, the low phonon energy modes are cut off in smaller particle sizes due to the phonon confinement effect, which reduces the energy transfer between a donor and an acceptor and significantly decreases the UCL.[27,28] It is reasonable to combine both factors when studying the size-dependent UCL. However, a recent work on the single cubic (α)-phase $NaYF_4$ based UC nanocrystals[23] argued that the phonon-mediated processes should be the reason for the size-dependent UCL after comparing their experimental results with those of the reported Y_2O_3 based UCNPs[26] and concluded that the surface effects should be excluded. Nevertheless, due to the difficulty in controlling the particle size, shape, and monodispersity, there have been few quantitative data and yet no consistent criteria to evaluate the size- and shape-dependent UCL in a broad size range. The

* Corresponding author. E-mail: jshan@princeton.edu. Phone: 1-609-2581411ú. Fax: 1-609-258-6109.
† Department of Mechanical and Aerospace Engineering.
‡ Princeton Institute for the Science and Technology of Materials.

10.1021/jp908976n
Published on Web 01/22/2010

experiments without well-defined particle size and shape and photophysical investigations without consistent criteria have led to debatable conclusions as above. Sometimes, it led to contrasting observations on a UC process. For instance, an opposite correlation between the green to red emission intensity ratio ($f_{g/r}$) and particle sizes was observed on the $NaYF_4$ based UCNPs.[22,23]

It was also reported that when the β-UCNP sizes were over 70 nm, $f_{g/r}$ became constant; therefore, the UC properties of the UCNPs larger than 70 nm were the same as those of the bulk UC phosphors.[22] We noticed that this observation was based on the UCNPs in different shapes, viz., the sphere or the prism shapes in smaller sizes (<45 nm) and the plate shape in larger sizes (to be discussed in more detail). As such, the shape-dependent UC properties have been largely overlooked. To our knowledge, the synthesis of size and shape controllable $NaYF_4$ based UCNPs during the past five years has been limited to a very narrow size range concerning the particle shape. For example, the size windows for the prism-shaped β-UCNPs were of 20−47 nm via a cothermolysis method[13] and 18−45 nm via a hydrothermal method.[12] Although a size range of 20−300 nm of the β-UCNPs was reported, the particles over 50 nm were actually in a different plate shape.[13] In many other literatures reporting the controllable synthesis of β-UCNPs, when UCNPs grew over 50 nm, the particle shape was inevitably changed.[12,13,29−32] Until recently, our group achieved synthesizing the consistent prism-shaped UCNPs in the range 18−200 nm.[15] In addition, we have also achieved the synthesis of rod-shaped β-UCNPs.[17]

In the present work, we report a systematic study of the effects of the particle size, shapes (prism and rod), and NP−ligand interface on the UCL properties of the β-$NaYF_4$:Yb,Er UCNPs with different aspect ratios (*W*/*L* or width/length) and SA/Vol ratios. For comparison, one of the plate-shaped UCNPs is also studied. We reveal the first observation of shape effects on the UCL and investigate the potential reasons besides the surface effects. Accordingly, aiming at clarifying the current contrast and contradictory observations on the UCL, three general criteria for assessing the UCL of UCNPs are proposed.

II. Experimental Section

Materials. Reagents of oleic acid (OA) (99%), trioctylphosphine (90%), octadecene (ODE) (90%), sodium trifluoroacetate (98%), and trifluoroacetic acid (reagent grade) were purchased from Sigma-Aldrich. Re_2O_3 (Re = Y, Yb, and Er) (99.99%) was provided by Sunstone Inc.

Synthesis. The hexagonal UCNPs in prism and rod shapes were synthesized according to our previous work.[15,17] The plate-shaped UCNPs were synthesized according to ref 11. The typical procedures toward differently shaped UCNPs are the following: Synthesis of OA-TOP coated β-$NaYF_4$:Yb,Er UCNPs was carried out using the standard oxygen-free procedures. OA-TOP capped UCNPs were prepared in the range 18−200 nm. For example, for 100 nm $NaYF_4$:Yb(20%),Er (2%) UCNPs, a mixture of 2.81 mmol of Na(TFA), 1.46 mmol of $Y(TFA)_3$, 0.375 mmol of $Yb(TFA)_3$, and 0.0375 mmol of $Er(TFA)_3$ was dissolved in OA/TOP/ODE (2 mL/2 mL/16 mL). Under vigorous stirring in a 50 mL flask, the mixture was first heated in an oil bath at 100 °C under a vacuum for 30 min to remove water, and then nitrogen was purged into the solution periodically. In the presence of nitrogen, the solution was then heated with a heating mantle to reflux temperature (~315 °C) within 10−15 min, and the reaction was stopped after 1 h of heating at reflux. The cooled solution was divided into two centrifuge tubes (45 mL) and added by ethanol (30 mL) to precipitate UCNPs. The UCNPs were isolated by centrifugation and were washed by excess ethanol at least three times. After washing, the product was left to dry at atmosphere and the yield was between 250 and 300 mg. Na/Re ratios were varied to prepare β-UCNPs in different size, and we found the yield was slightly increased with Na/Re ratios. Synthesis of the rod-shaped UCNPs was controlled by adjusting both Na/Re atomic ratios and OA/TOP volume ratios. Synthesis of the plate-shaped UCNPs was obtained by using OA as the only coordination ligand.

Characterization. TEM images of UCNPs were obtained using a LEO/Zeiss 910 TEM equipped with a PGT-IMIX EDX system (100 keV). With a field-emission gun, this microscope provides a point-to-point resolution of 0.2 nm and uses an electron probe of 0.7 nm with an energy up to 200 keV. A powder X-ray diffractometer (XRD, 30 kV and 20 mA, CuKα, Rigaku) was used for crystal phase identification. The powders were pasted on an alumina substrate, and the scan was performed in the 2θ range 10−70°. The energy dispersive spectrometer (EDS) analysis was performed using an FEI XL30 FEG-SEM instrument equipped with a PGT-IMIX PTS EDX system.

According to the literature methods,[33] the UCL intensities were measured on a thin solid sample pellet. The measurement setup is shown in Figure S1 of the Supporting Information. To be consistent for the whole measurements, a hole on a copper substrate with a 0.5 mm depth and 6 mm diameter was built to accommodate the samples. A copper substrate was selected due to its high heat conductivity, which minimized the thermal effects during the measurements. The samples were excited using a Thorlabs F240FCB collimated Qphotonics 975 nm diode laser, driven with a Thorlabs LDC3065-488 High Power Laser Diode Driver. The beam was focused (50 mm focal length) on a spot size of approximately 1 mm in diameter. The UCL signal was focused again by a spherical lens and then collected by a monochromator (SP-2500i, Princeton Instruments) with a 2400 g/mm grating (holographic, 400−700 nm). The signal was detected by a photomultiplier module (H6780-04, Hamamatsu) and was amplified by a lock-in amplifier (SR510, Stanford Research Systems) together with an optical chopper (SR540, Stanford Research Systems). The signal was recorded under computer control using the SpectraSense software data acquisition/analyzer system (Princeton Instruments, Trenton, NJ). When comparing the UCL intensities of the differently sized and shaped UCNPs, the same excitation power has been used to excite the samples.[12,19,23,34] Due to the nonlinear photophysical properties in UCNPs, and more importantly, the radiative and nonradiative energy cross relaxations among the f-orbitals are excitation power and size dependent, the quantum efficiency data for either green or red emissions do not represent the exact photoluminescence (PL) efficiency and are therefore not used here for assessing the UC efficiency.

The dynamic luminescence decay measurements were conducted with a Qphotonics diode laser (QSP-975-6) driven by an EO Devices ETX-10A-C 5 V with pulses generated by a Directed Energy (PDG-2515) pulse generator. The luminescence lines were filtered by a monochromator (Jobin Yvon) before detection by a Hamamatsu R6095 PMT connected to a preamplifier. The decay curves were collected by a 500 MHz Tektronix Digital Oscilloscope (TDS3052B) with averaging (512 cycles). The laser pulse was 1 ms width at 10 Hz, and the rise time of the photodetector is less than 15 ns (Hamamatsu R6095 PMT). The laser pulse rising and fall times are less than 1 ns. The measured decay times were on the order of hundreds of microseconds. Since the range of decay time was 5 orders of magnitude higher than the response time of the detector, deconvolution was not needed.

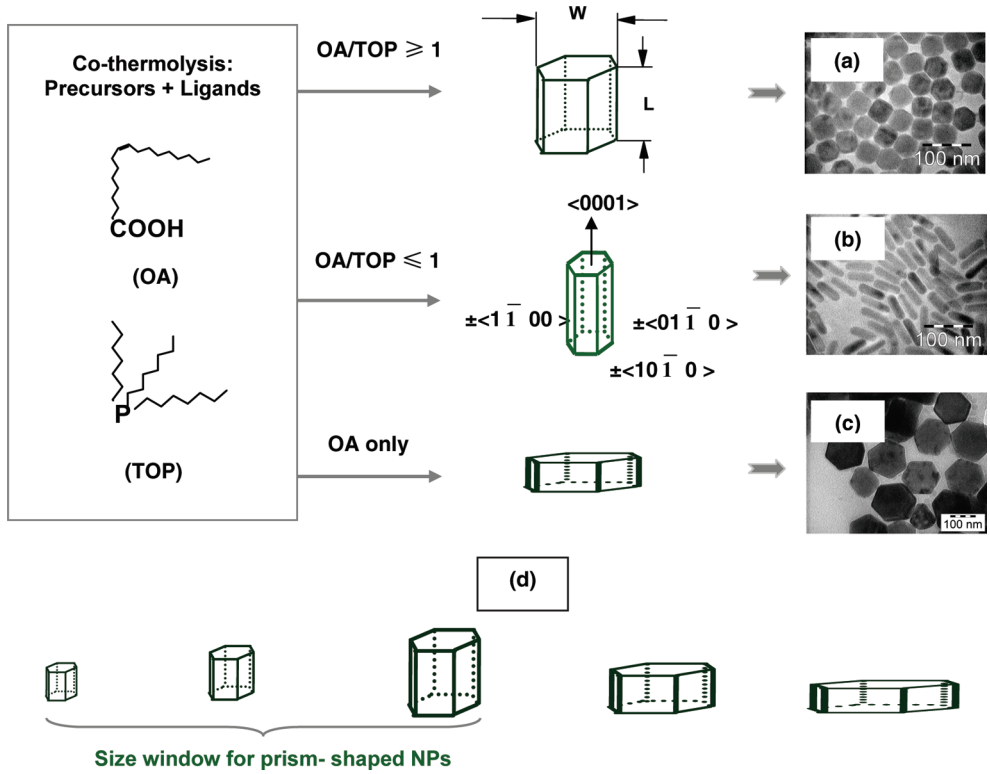

Figure 1. Schematic structures, crystal planes, TEM images of the UCNPs in three shapes (a−c) and (d) description of the size window.

III. Results and Discussion

A. β-UCNPs with Different Sizes and Shapes and Size Window. Figure 1 shows the schematic of the three particle shapes for β-UCNPs, three corresponding TEM images, and the description of the size window for prism-shaped UCNPs. In this work, the particle width (W) and length (L) were counted by averaging the corner-to-corner distance of the hexagonal surface and the distance between the top and bottom, respectively (Figure 1a). For prism-shaped UCNPs, the W/L ratio is close to unity. When they were self-assembled on the copper grids for 1-D transmission electron microscopy (TEM) characterization, the hexagonal or square morphologies representing the W or L side were then in a random distribution (Figure 1a and Figure S2 of the Supporting Information). For plate or rod-shaped UCNPs, either W or L, whichever is larger, is shown in TEM images (Figure 1b,c and Figure S3 of the Supporting Information). More TEM images of the UCNPs, sample monodispersity histogram, and arrows showing the calculations of W and L values are shown in Figures S2 and S3 of the Supporting Information. The crystal planes of a β-crystal with the typical top/bottom $\langle 0001 \rangle$ (c-axis) and six equivalent $\langle 10\bar{1}0 \rangle$ families (a-axis), consisting of $\pm\langle 1\bar{1}00 \rangle$, $\pm\langle 01\bar{1}0 \rangle$, and $\pm\langle 10\bar{1}0 \rangle$, are also shown (Figure 1b). SA and Vol of the β-UCNPs are calculated using averaged W and L values and assuming that all of the individual nanocrystal is in an ideal hexagonal structure.

We noticed that when the literature counted the sizes of β-UCNPs in plate or rod shapes, usually both W and L had been applied. However, when correlating the size-dependent UCL, it is unclear which length should be counted. For instance, for the as-reported 70 and 185 nm UCNPs, the actual $W \times L$ values were 72.1 nm × 45.5 nm ($W/L = 1.60$) and 185 nm × 75 nm ($W/L = 2.47$), respectively.[22] In the subsequent photophysical investigations, not only was the shape effect not considered in the size calculation, but also the size-dependent observations were not considered; e.g., the UC properties of the UCNPs over 70 nm were found to be similar to those of the bulk materials. The prism-shaped UCNPs selected for this study with W/L ratios between 1.04 and 1.10 ($W = 35-150$ nm, Table 1) address the incomplete investigation stated above. We also achieved the prism-shaped β-UCNPs with the W values of 18 and 190 nm (not shown).[15] Considering that the rod- or plate-shaped UCNPs have various W/L aspect ratios and meanwhile in order to evaluate the UCL of the differently shaped UCNPs with a same standard, the SA/Vol ratios instead of the particle sizes are then used. Table 1 summarizes the sizes, shapes, W/L, SA/Vol ratios, and ion compositions of all the UCNPs in this work. Representative EDS and XRD patterns are given in Figure S4 of the Supporting Information.

TABLE 1: Summary of the Differently Sized and Shaped UCNPs[a]

UCNPs	W (nm)	L (nm)	W/L	SA/Vol	Yb/Er (at. %)	shape
1	150.5	136	1.10	0.030	23.3/1.5	prism
2	107.4	99.6	1.08	0.042	26.7/2.0	prism
3	67.7	63.5	1.07	0.066	29.0/2.1	prism
4	48.0	46.0	1.04	0.092	24.8/2.0	prism
5	38.7	36.7	1.05	0.114	30.2/1.9	prism
6	66.7	120	0.56	0.051	21.3/2.5	rod
7	53.3	83.3	0.64	0.067	20.6/1.7	rod
8	44.5	66.7	0.67	0.082	31.0/1.9	rod
9	20.1	60.7	0.33	0.15	21.3/1.6	rod
10	18.3	36.7	0.50	0.18	27.1/1.6	rod
11	142.9	65.3	2.19	0.047	20.1/2.1	plate

[a] Particle sizes were counted over 200 particles from TEM images. For samples 1 and 2, errors of counting W and L are ±2.5 nm; for samples 3−11, errors are ±0.6 nm. SA/Vol ratios were calculated assuming that the individual nanocrystal is an ideal hexagonal structure. Errors for SA/Vol are <1%.

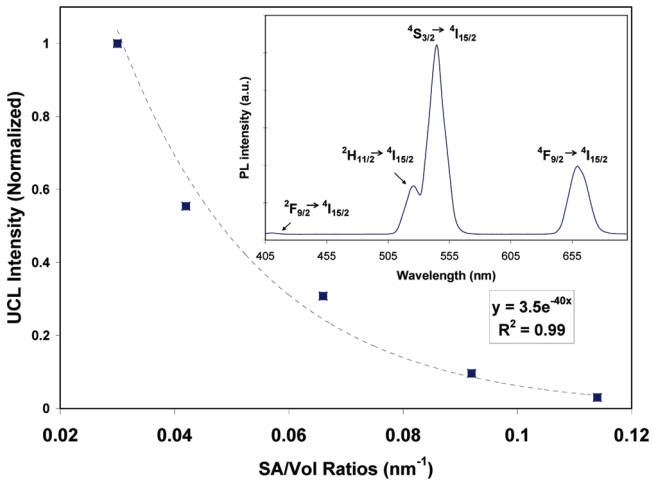

Figure 2. UCL intensity vs SA/Vol and UC emission spectrum (inset).

SCHEME 1: Energy-Level Diagram of Yb^{3+}/Er^{3+}-Codoped UCNPs and UC Processes under 978 nm Excitation

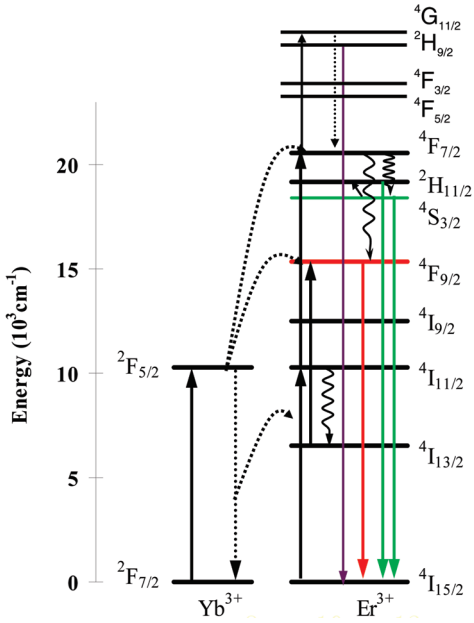

B. UCL Intensity as a Function of SA/Vol Ratios and Shape Effects. The UCL intensity of the five prism-shaped UCNPs as a function of the SA/Vol ratio and emission spectrum of sample 1 (inset) are shown in Figure 2. The UC mechanism and population processes in Yb^{3+}/Er^{3+} codoped systems are presented in Scheme 1. The two green emissions between 510 and 560 nm (Figure 1, inset) are attributed to the transition from $^2H_{11/2}$ and $^4S_{3/2}$ levels (Er^{3+}) to the ground state of $^4I_{15/2}$, respectively. The emission between 635 and 685 nm is attributed to the transition of the $^4F_{9/2}$ level (Er^{3+}). A weak emission near 400 nm belongs to the $^2H_{9/2} \rightarrow {}^4I_{15/2}$ transition. Since all of the prism-shaped UCNPs have comparable Yb/Er ratios (Table 1), the exponential UCL increase with the decrease in SA/Vol ratios could be correlated with the surface properties at the interface between the UCNP and coordination ligands. Ligand effects and surface Er^{3+} ion fraction have been proposed to account for the size-dependent UCL performance on the OA ligated UCNPs,[22] which can also be applied to give a qualitative explanation on the OA-TOP ligated UCNPs in our work. First, the UCNPs with high SA/Vol ratios (small particles) usually

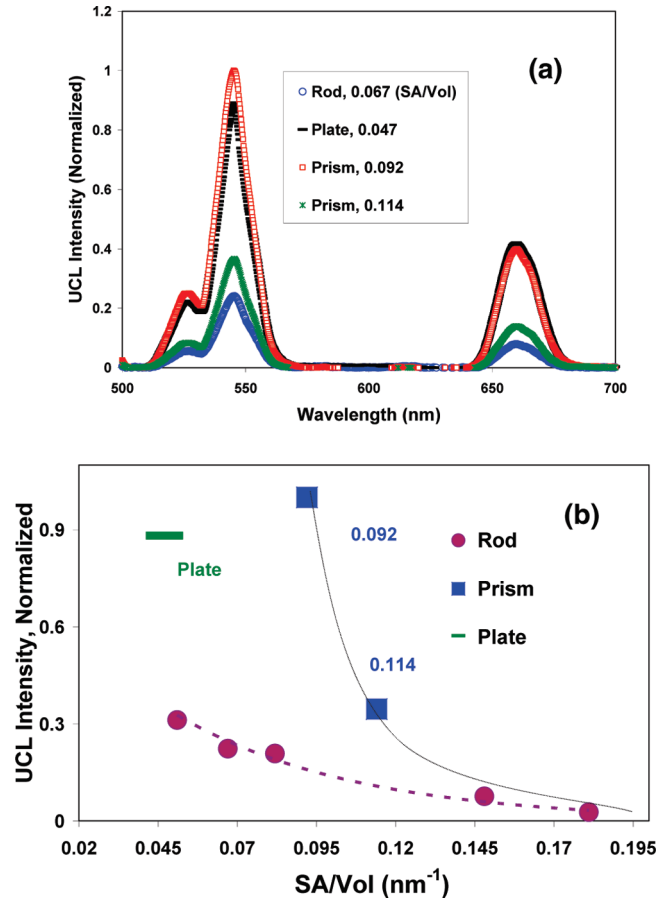

Figure 3. (a) UC emission spectra and (b) SA/Vol ratios vs UCL intensity for differently shaped UCNPs.

have more surface defects and Er^{3+} ion fraction on the particle surface, which cause the enhanced nonradiative quenching and result in the diminished UCL. As for ligand effects, they are coordinated to the surface Er^{3+} ions. More surface ions increase the ionic properties between the NP and ligands; as a result, the small NPs have more quenching sites than those of the large NPs and reduce UCL intensity. An additional proof of the ionic property induced by the ligand coordination and Er^{3+} ions could be seen directly from the physical states of our UCNPs. The small OA-TOP ligated UCNPs usually are more rigid and powder-like, while the large UCNPs are more sticky and easier to be dissolved in organic solvent (e.g., hexane).

From Figure 2, there is no threshold particle size differentiating the UCL in the size range from 37 to 150 nm (averaging *W* and *L*). A size boundary of 70 nm between nanoscale and bulk state[22] was not observed in this work. The reason is most probably due to the β-UCNPs studied in ref 22 are not in a consistent shape and the excitation power selection (to be discussed in section E). The major difference between our prism-shaped and literature plate-shaped UCNPs is the *W*/*L* aspect ratios. This inspires us to explore more of the shape effect. Under the assumption of the absence of a shape effect in UCNPs, the UCL of the differently shaped UCNPs is expected to fit into the prism-shaped UCNPs in terms of the SA/Vol ratios. To test this, the UC emission spectra of the five rod- and one plate-shaped UCNPs are compared in Figure 3a. In Figure 3b, the UCL intensities of the five rod-shaped UCNPs (samples 6−10 in Table 1) are compared with the two prism-shaped UCNPs (samples 4 and 5) and one plate-shaped UCNP (sample 11) as a function of SA/Vol ratio.

The results in Figure 3 show that the UCL intensities of the five rod-shaped UCNPs also decrease with the increase of SA/Vol ratios, but not as significantly as those of the prism-shaped UCNPs. At the similar SA/Vol ratios, especially at the small SA/Vol ratios, the UCL intensities of the prism-, rod-, and plate-shaped UCNPs differ significantly. For example, although the prism-shaped UCNPs (sample 4) have ca. 2 times larger SA/Vol than that of the plate-shaped UCNPs (0.092 vs 0.047), their UCL intensity is still higher (1.1 times). Meanwhile, both of these UCNPs have much higher UCL (>3 times) intensities than those of the rod-UCNPs with a SA/Vol ratio of 0.051. The above results indicate that the SA/Vol ratio is a good standard to evaluate the UCL of the prism-shaped UCNPs with *W*/*L* aspect ratios close to unity, whereas for the differently shaped UCNPs with variable *W*/*L* aspect ratios, the SA/Vol is not enough to describe and compare the UC properties.

To confirm the shape effect, we conducted power-dependent UCL, green to red ratios ($f_{g/r}$), and dynamic luminescence decay and compared the UC processes in the prism- and rod-shaped UCNPs.

C. Power Dependence, Green to Red ($f_{g/r}$) Ratios, Dynamic Luminescence Decay, and NP−Ligand Interface. Pollnau et al. have shown that the UCL intensity (I) as a function of the excitation power (I_{IR}) is determined by the competition between the linear decay and UC processes for the depletion of the intermediate excited states, which can be expressed in eq 1.[25]

$$I \propto I_{IR}^{n} \tag{1}$$

where n is the number of IR photons absorbed per visible photon emitted. The two-photon UC mechanism (see Scheme 1 also) described here as an Yb^{3+} ion in ground-state $^2F_{7/2}$ absorbs a photon and transits to excited-state $^2F_{5/2}$, and then, the second 980 nm photon transfers the energy from an Yb^{3+} ion to populate the $^4F_{7/2}$ level of the Er^{3+} ion via an ETU process. This energy can then relax nonradiatively to the $^2H_{11/2}$ and $^4S_{3/2}$ levels, and the green $^2H_{11/2} \rightarrow {}^4I_{15/2}$ (525 nm) and $^4S_{3/2} \rightarrow 4I_{15/2}$ (545 nm) emissions occur. Alternatively, the Er^{3+} ion can further relax and populate the $^4F_{9/2}$ level, leading to the red emission of $^4F_{9/2} \rightarrow {}^4I_{15/2}$ (660 nm). Sometimes, the first absorbed phonon from the Yb^{3+} ion drops back to the ground state while transferring the energy to an adjacent Er^{3+} ion, which populates the $^4I_{11/2}$ level from the ground-state $^4I_{15/2}$. The energy can relax nonradiatively to the $^4I_{13/2}$ level. The ions in this level are excited to the $^4F_{9/2}$ state via the energy transfer from Yb^{3+} ions, which account for the partial three-phonon process observed in red emissions for some samples. As the excitation power is low, the linear decay is dominant and n usually equals 2 or is between 2 and 3, which indicates a two or mixed two and three photon UC process, respectively. As the excitation power is increasing, the UC process is dominant, n gradually becomes 1, and the UCL saturation appears. When n is smaller than 1, the UCL quenching due to the thermal effects results. The log−log curves of UCL intensity as a function of excitation power of the four prism- and two rod-shaped UCNPs are plotted in Figure 4.

It can be seen that the four prism-shaped UCNPs have n values (green emission) between 2.0 and 2.2 at the low excitation power without showing a dependence on the NP sizes or SA/Vol ratios. Hence, the UC process for green emission is the typical two-photon mechanism in which an Yb^{3+} ion in ground-state $^2F_{7/2}$ absorbs a photon and transfers to the excited-state $^2F_{5/2}$. The photon energy is transferred to an adjacent Er^{3+} ion, which populates the $^4I_{11/2}$ level from the ground-state $^4I_{15/2}$ via the ETU process. After that, a second 980 nm photon, or a photon at the energy level of $^2F_{5/2}$ in an Yb^{3+} ion, can populate the $^4F_{7/2}$ level in the Er^{3+} ion. The Er^{3+} ion can then relax nonradiatively to the $^2H_{11/2}$ and $^4S_{3/2}$ levels via multiphonon processes; as a result, the green emission occurs from $^2H_{11/2}$ and $^4S_{3/2}$ transitions to $^2I_{15/2}$. For red emission, Figure 4a−d shows that the slopes (n values) of the UCL intensity (average number of photons involved in the UC process) decrease monotonically from 2.6 to 1.8 with the decrease of SA/Vol ratios from 0.114 (sample 5) to 0.030 (sample 1); at large SA/Vol ratios (samples 4 and 5), the red emission has partly involved a three-photon upconversion process. This is probably due to the increasing surface defects on the small NPs resulting in nonradiative transition from $^4I_{11/2}$ to $^4I_{13/2}$; then, the electrons at the $^4I_{13/2}$ level need to absorb another photon via an excited state transition or undergo a cross relaxation ($^2F_{7/2}$, $^4I_{13/2}$) to $^2F_{9/2}$ and emit red emission from the following $^2F_{9/2}$ to $^2I_{15/2}$ radiative transition.

As for the two rod-shaped UCNPs (Figure 4e and f), the green emissions show a two-photon process at low excitation power (slope = 2.3 and 2.1, respectively). However, for red emission, the dependence of the UC process on the SA/Vol ratio is opposite to that of the prism-shaped UCNPs. The red emission of the UCNPs with lower SA/Vol presents a mixed two and three photon process (n = 2.6). The results from other rod-UCNPs also confirm this observation.

Another important UC property is the intensity of green to red emission ($f_{g/r}$) ratios, which indicate the variations of radiative and nonradiative relaxation for either green or red emission in an Er^{3+} environment. Suyver et al. have reported that the $f_{g/r}$ of the bulk UCNPs was strongly dependent on the excitation power.[10] In this work, we examine whether this conclusion also applies to the nanosized UCNPs with different sizes and shapes. Figure 5 shows excitation power density vs $f_{g/r}$ ratios of the UCNPs in Figure 4. The saturation powers and $f_{g/r}$ values at the saturation points, which are determined approximately at the intersection of the $n \sim 2$ and $n \sim 1$ as shown in Figure 5a, are also shown.

Figure 5a−d shows that the saturation powers of the prism-shaped UCNPs decrease with the reduction of the SA/Vol ratios, which can be explained as the UCNPs increase in size (smaller SA/Vol ratio), more dopant ions are located inside the bulk of the crystals and therefore enhance the energy transfer between the dopant ions with a more efficient UC process taking place. The β-UCNPs with larger SA/Vol ratios, on the other hand, usually have more dopant ions exposed on the crystal surface and a reduced number of interactions between neighboring ions. This subsequently diminishes the energy transfer between Yb^{3+} and Er^{3+} ions, thereby reducing UC efficiency and increasing the saturation power.

From Figure 5, it can be seen that all of the UCNPs except sample 9 (small rod) show the observable of the decreasing $f_{g/r}$ ratios with increasing excitation power, which is similar to the observation on the bulky β-UCNPs.[10] When approaching the saturation power, for the four prism-shaped UCNPs, there are no significant differences in $f_{g/r}$ ratios (between 1.61 and 1.77), while the two rod-shaped UCNPs present $f_{g/r}$ ratios of 3.13 and 2.12 for the SA/Vol ratios of 0.15 and 0.067, respectively, which are higher than those of the prism-shaped UCNPs. These results suggest that, in the prism-shaped UCNPs, the cross relaxation from $^4F_{7/2}$ to $^4F_{9/2}$ is more effective than that in the rod-UCNPs, causing an increase of $f_{g/r}$ ratios. It is interesting to see that the rod-UCNPs in high SA/Vol (0.15, sample 9) do not present significant excitation power-dependent $f_{g/r}$ ratios under the power strength used in this work, which is also observed on the rod-

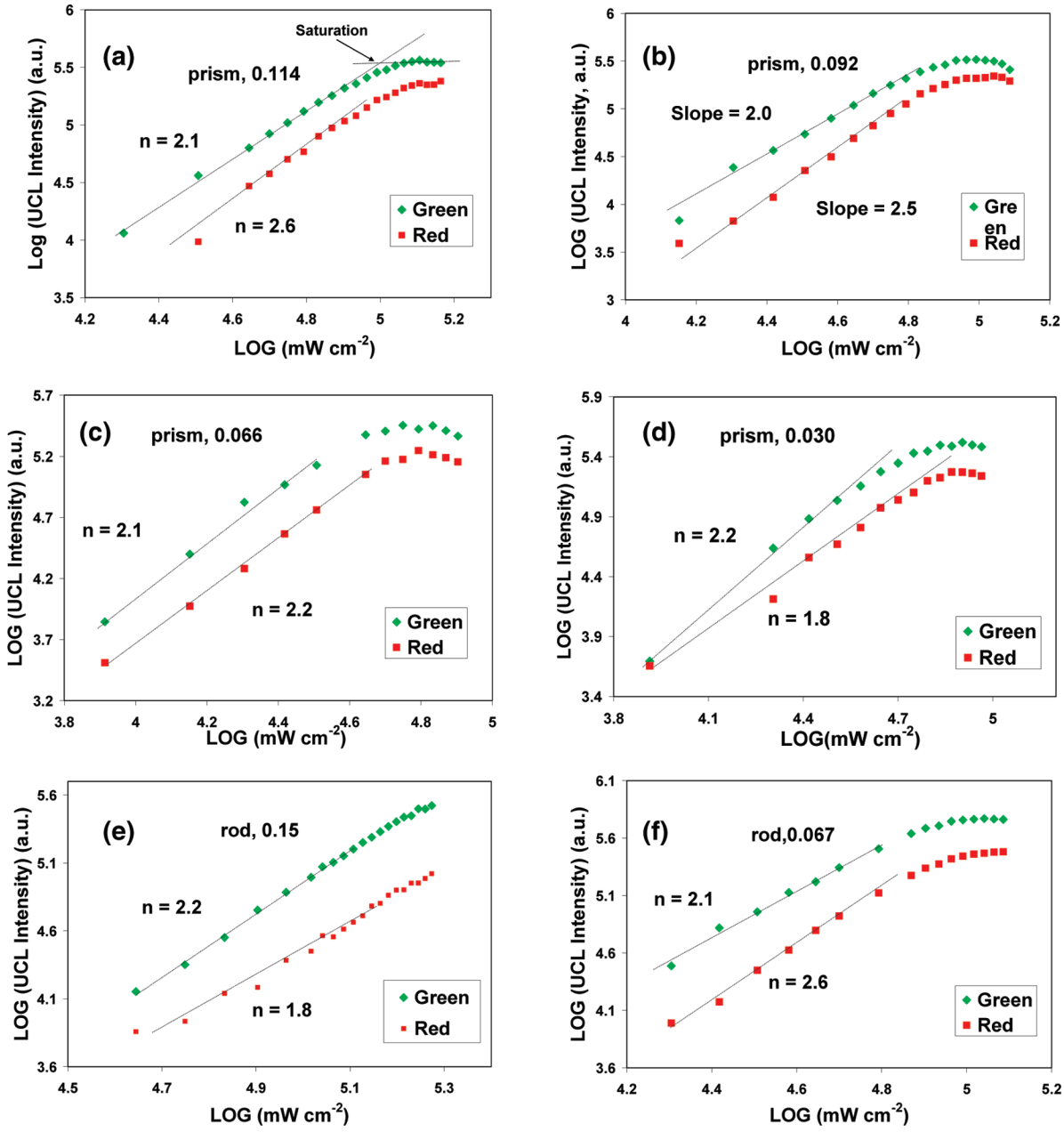

Figure 4. Log−log diagrams of green and red luminescence intensities: (a−d) for prism UCNPs of samples 5, 4, 3, and 1 in Table 1; (e and f) for rod UCNPs of samples 9 and 7 in Table S1 of the Supporting Information.

shaped UCNPs with even higher SA/Vol (0.18, sample 10, $f_{g/r}$ = 3.5, not shown). We did not increase the power further, since the thermal effects would be in effect and potential sample annealing on changing the particle size could appear.[35] We measured the temperature of the copper substrate at the saturation excitation power (sample 5), which was around 35 °C. In another experiment, we heated the substrate and collected spectra by using a low excitation power. We found that the $f_{g/r}$ ratios of the UCNPs had insignificant differences between the room temperature and at 40 °C. To reach the same $f_{g/r}$ ratio as that in the saturation power, the copper needed to be heated to around 80 °C (data to be reported elsewhere); therefore, the temperature effects induced by the excitation power were not considered in this work for $f_{g/r}$ comparison.

The $f_{g/r}$ ratios of the prism- and rod-UCNPs with SA/Vol ratios of 0.066 and 0.067, respectively, are directly compared in Figure S5 of the Supporting Information. It can be seen that the rod-UCNPs present systematically higher $f_{g/r}$ ratios than those of the prism-UCNPs. This and the above power-dependent UCL results suggest that the surface effects are not enough to explain the UC properties, while the shape effects should be considered.

To have more convincing proof of this shape effect, the luminescence dynamics that depends critically on the phonon density of states in the nanocrystals[27,28] was performed on the three prism- and three rod-shaped UCNPs from Table 1. Figure 6a shows the dynamic fluorescence (543 nm) decay curves, and Figure 6b compares the decay lifetimes as a function of SA/Vol ratio. For the prism-UCNPs, the smaller the SA/Vol ratios are, the longer the decay times, and there is almost a linear relationship between the decay times and SA/Vol ratios. However, for the rod-UCNPs with SA/Vol = 0.051, its decay time (283 μs) is shorter than that of the prism-UCNPs with SA/Vol = 0.066 (387 μs). Interestingly, the decay times of the three rod-UCNPs slightly increase (283, 313, and 374 μs) with increasing SA/Vol ratios (Figure 6b). These results are not unexpected, since, different from the prism-UCNPs that have a

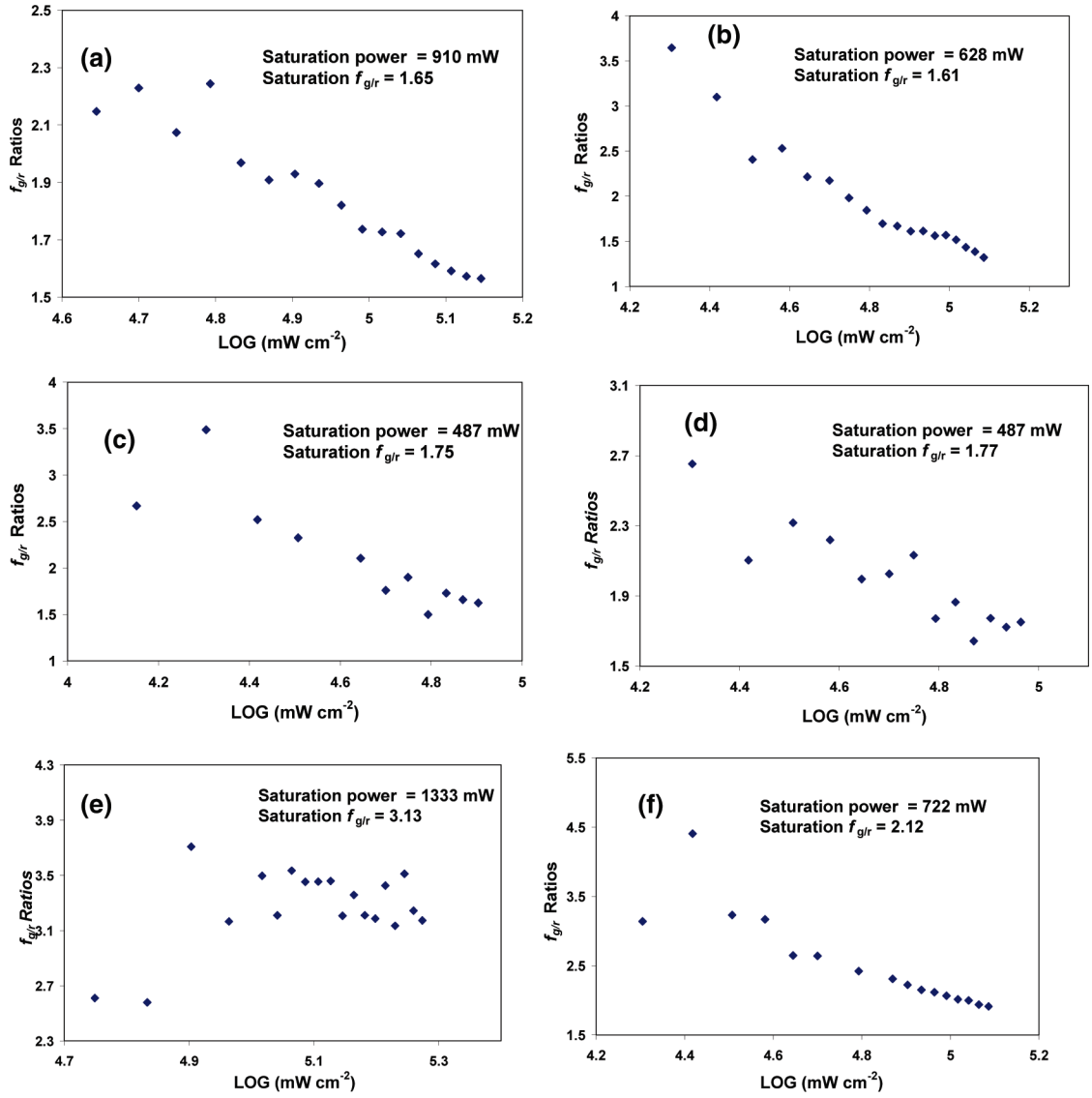

Figure 5. Saturation powers and excitation power density vs $f_{g/r}$ ratios. Samples are in the same order as those in Figure 4.

constant *W*/*L* aspect ratio ($\sigma < 5\%$), the *W*/*L* ratios of the three rod samples increase from 0.56 to 0.67 (more *W* sides) ($\sigma \sim 20\%$) with the increase of SA/Vol ratios. The information from the dynamic fluorescence decay strongly indicates that the differently shaped NPs with the different *W*/*L* aspect ratios and different fractional lattice compositions (more *W* or more *L* side components) should have different phonon relaxation processes (to be discussed further in the next section). Indeed, this and all of the above characterization data show the different Er^{3+} environment of the differently shaped UCNPs and the shape effects on the UCL. A more detailed dynamic investigation of the rising and decay lifetimes correlated to the phonon confinement on these differently sized and shaped UCNPs is currently underway.

Lastly, a control characterization is necessary to investigate the vibrational energies at the interface of the inorganic (NP) ligands of both the rod- and prism-UCNPs. Figure 7 shows the IR spectra of the two differently shaped β-UCNPs with the similar SA/Vol ratios. Both UCNPs have strong vibrational energies at ~2940 and 1720 cm^{-1} due to the alkyl-containing coordination ligands. The results do not show observable shape-dependent vibrational energies and therefore exclude that the surface effects are the only reason responsible for the UCL properties. More discussion on those vibrational energies is in the following section.

D. Discussion of the Shape Effect. As mentioned earlier, under the comparable conditions of host matrix, crystalline phases, dopant concentrations, and activator (Yb^{3+}) to acceptor (Ln^{3+}) concentration ratios, the surface effects and restricted phonon relaxation at higher frequencies have been used to explain the decrease of the UCL with the reduction of the particle sizes (or increasing SA/Vol ratios).[22,27] The surface effects based on the SA/Vol ratios well explain the experimental data of the prism-shaped UCNPs but cannot be generalized to other-shaped UCNPs in our work. Under the mode of restricted phonon relaxation at a small particle length scale, the UCL and dynamic luminescence decay data indicate that the rod-UCNPs might have more reduced multiphonon relaxation for both green and red emissions than those of the prism-shaped UCNPs. By analyzing the crystalline axes of the prism- and rod-shaped β-phase crystals, a qualitative explanation on the shape effects can be given by comparing the *d*-space distances between the crystal planes and axis components. The calculated lattice constants for the β-$NaYF_4$ crystals are, respectively, $a = 0.5991$ nm and $c = 0.3526$ nm,[8] which match the measured *d*-spacing values of $\langle 10\bar{1}0 \rangle$ and $\langle 0001 \rangle$ families with ~0.51 and ~0.36

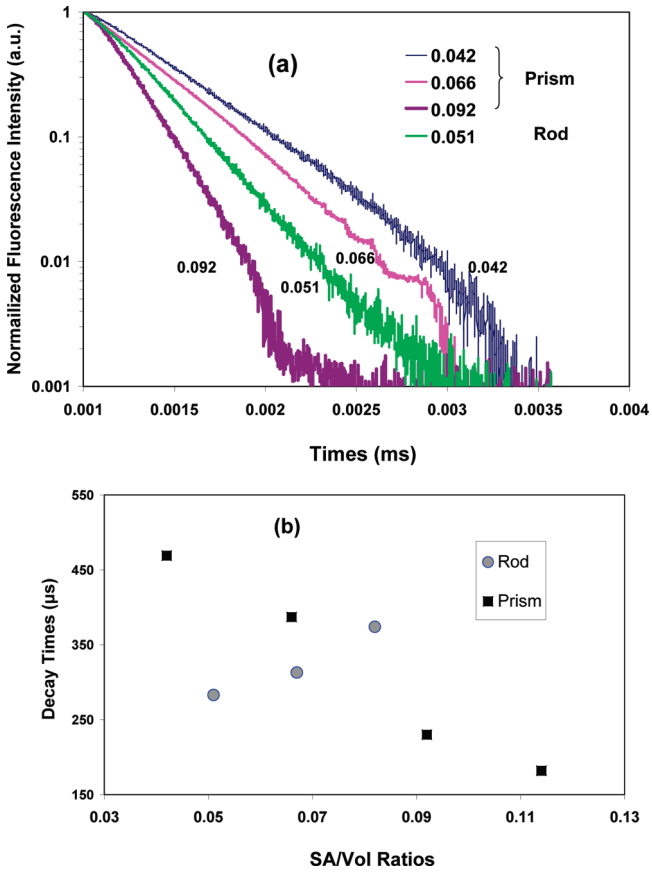

Figure 6. Fluorescence decay times at 543 nm of the prism and rod-UCNPs: (a) decay spectra; (b) decay times as a function of SA/Vol ratios.

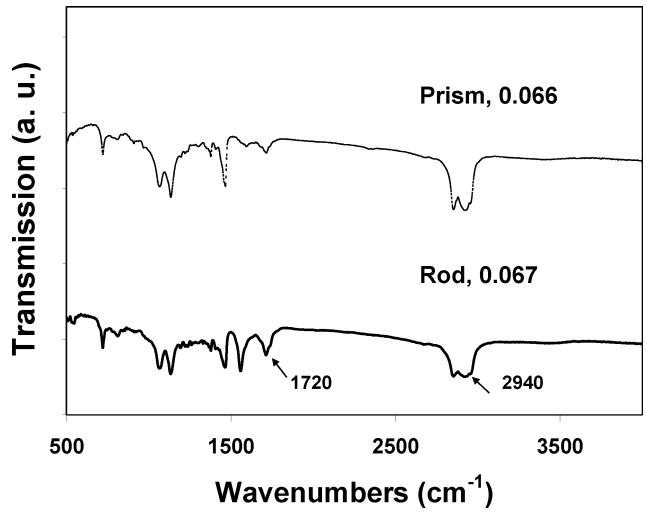

Figure 7. NIR spectra of the prism- and rod-shaped UCNPs with similar SA/Vol ratios.

nm in the β-UCNPs,[13] respectively. Hence, the rod-UCNPs prefer the *c*-axis growth and have higher fractions of ⟨0001⟩ packing planes than those of the prism- and plate-shaped UCNPs. As a result, the mean distance between ions becomes smaller. The lattice energy of ionic crystals u_{coul} at the distance r amounts to $u_{coul} = -(1/4\pi\varepsilon_0)(Z^2e^2/r)$, where ε_0 is the vacuum permittivity.[36] Therefore, the crystal lattice r has a significant effect on the lattice phonon energy and the energy transfer between the ions. In future research, more quantitative measurements, such as the temperature-dependent excitation spectra[27] or Raman spectra on UCNPs with different shapes can be applied to investigate the shape dependence on phonon-energy distribution and potential confinement of the optical phonons along the short *c*-axis of the rod-shaped particles. On the other hand, another possible explanation could be due to the fact that the shorter crystalline plane distance and larger fractions of ⟨0001⟩ packing planes increase the inter ion−ion cross relaxation and energy back transfer from Er^{3+} to Yb^{3+}.[22] In both cases, the UCL is decreased. The UCL data in the previous sections showing the shape effects on UCL intensity, saturation powers, $f_{g/r}$, and dynamic luminescence decay can be explained accordingly.

Note that the nanoparticles growing in the direction of the *c*-axis with decreased photoluminescence were also observed on the rod-shaped CdSe nanocrystals.[37] The work performed by Peng et al. showed a much lower quantum yield of the rod-CdSe (wurtzite, $c/a = 9.1/4.5$ nm/nm) than that of the dot-shaped CdSe ($c/a = 5.6/4.2$ nm/nm). The *c*-axis is thought to be dark due to the unique-axis polarized emission in the study of the quantum dots.[38] In our work, the prism-UCNPs (SA/Vol = 0.066) have nearly 5 times the UCL intensity as that of the *c*-axis rich rod-UCNPs (SA/Vol = 0.067). This diminished photoluminescence in the rod-shape phosphors was also observed in the $NaYF_4$:Eu NPs ($c/a = 36/25$ nm/nm, photoluminescent intensity 1.5 times lower) in comparison with the sphere-shaped NPs ($c/a = 19/19$ nm/nm).[11] It should be noted that the differences in the photophysical properties between the lanthanide doped NPs and quantum dots are significant. For lanthanides, the spectroscopically active 4f electrons are well shielded from their chemical environments by the outer-lying 5s and 5p electrons; therefore, the electron−phonon coupling strengths for lanthanides are much weaker than those in the quantum dots. Nevertheless, both nanocrystals have an anisotropic orientational crystalline growth direction (*a*-axis and *c*-axis). As such, the physical understandings gained in the studies of quantum dots could be applied to explain the experimental observations of the lanthanide doped NPs. The future study of the similarity and potential connections between the two differently typed nanocrystals could bring much theoretical interest from the physical insights.

E. Criteria for Evaluating the Size-Dependent UCL. On the basis of our photophysical characterization data and identification of the shape effect, in order to address the contradictory observations reported in the literature, we propose three general criteria: (i) a broad particle size window with a consistent shape, (ii) a systematic investigation of $f_{g/r}$ as a function of the excitation power, and (iii) comparable UC hosts and surface properties to study the size-dependent UCL of the UCNPs.

The first criterion is required because the lanthanide doped NPs are the insulators without quantum size effects. Unlike quantum dots that have a Bohr radius usually smaller than 10 nm, a small size change (~0.1 nm) can shift energy band gaps and fluorescence peak positions and alter the quantum yields.[39] However, for Yb^{3+},Er^{3+} doped UCNPs, the emission peaks have little change at room temperature due to the f−f orbital transition and the size change of a few nanometers does not shift the UCL spectra and intensity dramatically. As a result, for a given crystal shape, the surface effect is proportional to the SA/Vol ratios and a broad size range is needed to observe and study the size-dependent UCL. On the other hand, since the *W*/*L* aspect ratios of the UCNPs can affect the UCL intensities, the particle shape needs to be considered. We believe that a size window for the prism-shaped UCNPs over 100 nm (either *W* or *L*) is more suitable for the study of the size-dependent UCL properties.

This criterion also applies to other hosts such as Y_2O_3 based UCNPs with unequal lattice constants.

The second criterion is required to clarify the contradictory observations on $f_{g/r}$ vs particle sizes reported on the Y_2O_3 and $NaYF_4$ based UCNPs. Previous studies have observed the increasing $f_{g/r}$ ratios with the increase of particle sizes on the Y_2O_3:Yb,Er UCNPs (12−65 nm).[26] In contrast, the decreasing $f_{g/r}$ ratios with the increase of particle sizes was found on the single α-$NaYF_4$:Yb,Er nanocrystals (5.6−65 nm).[23] Our results show that comparing the UC processes of the differently sized UCNPs by collecting the $f_{g/r}$ ratios at only one or two excitation powers is not accurate. In this work, taking the 37.0, 47.0, 65.6, and 143.3 nm (averaging *W* and *L* for the samples 5, 4, 3, and 1 in Table 1, respectively) prism-UCNPs, for example, the $f_{g/r}$ ratios are 2.24, 1.84, 1.77, and 1.77 at an excitation power of ∼60 W/cm^2 (LOG (mW/cm^{-2}) ∼ 4.8), respectively. However, as shown in Figure 4, at this excitation power, the ETU process of the 37.0 and 47.0 nm UCNPs is dominated by the linear quenching. The 65.6 nm UCNPs are dominated by the UC process. The largest 143.3 nm UCNPs are already at the saturated UC regime. As shown in Figure 5 and Figure S5 of the Supporting Information, our results show a decreasing $f_{g/r}$ with the increase of the excitation power for all of the samples. At high excitation power (saturated) for each sample, the $f_{g/r}$ ratios are very close (1.61−1.77) for prism-shaped UCNPs, indicating the same ETU process for these UCNPs. This observation might explain why the same $f_{g/r}$ ratios were observed on the OA coated β-UCNPs after the sizes exceeded 70 nm,[11] which could be due to the fact that the excitation power applied to excite the large UCNPs was already saturated. Therefore, a systematic investigation of $f_{g/r}$ as a function of the excitation power would be more suitable to investigate and compare the UC properties of the UCNPs with different sizes. Our results show that the $f_{g/r}$ ratios are inversely related to the UCNP sizes at a low excitation power, which are the same as the literature observations (ref 23) on the single cubic (α)-phase $NaYF_4$ UCNPs. However, the literature results (both refs 23 and 26) still failed to identify the ETU stage at each excitation power.

Interestingly, the relationship between the $f_{g/r}$ ratios and particle sizes of the Y_2O_3:Yb,Er UCNPs in ref 26 was opposite the literature report of ref 23 and our results. The study of fluoride UCNPs in ref 23 denied surface effects on the $f_{g/r}$ and UC process according to the opposite observation. We noted that the two UCNPs were prepared from different routes and had totally different surface properties as well as the lattice phonon energy. It has been counted that populating the green ($^2H_{11/2}$) and red ($^4F_{9/2}$) emitting levels needs energy gaps of 2000 and 5000 cm^{-1} from $^4F_{7/2}$,[23] respectively. First of all, the Y_2O_3 lattices have a higher phonon energy than that of $NaYF_4$ (597 cm^{-1} vs 360 cm^{-1}),[10,40] and a large lattice phonon energy is usually helpful to bridge the larger gap for red emission. Second, we believe that the surface effects still play crucial roles in affecting the $f_{g/r}$ ratios of both UCNPs. The as-prepared Y_2O_3 UCNPs in ref 26 were sent to high temperature annealing (>500 °C), and therefore, OH^{-1} groups would be the dominant species on the particle surface during the UC measurements; while the $NaYF_4$ based UCNPs in ref 23 were prepared using *N*-(2-hydroxylethyl)ethylendiamine ligands via a colloidal synthesis,[41] the as-prepared UCNPs should have vibrational relaxations at the inorganic−ligand interface similar to our work (2940 and 1720 cm^{-1}) shown in Figure 7. For OH^- groups on Y_2O_3, the vibrational energy is ∼3400 cm^{-1}. Hence, the Y_2O_3 UCNPs should have higher fractions of red emission due the fact that their surface vibrational energies are closer than those of the alkyls to bridge the nonradiative relaxation gap for red emission. As discussed earlier, as the particles become smaller in nanoscale, there will be more Er^{3+} locating at the NP surface, and therefore there are more surface vibrational sites to support the red emission than the green emission. While for the $NaYF_4$ based UCNPs, besides the strong vibrational energy peaks around 2940 cm^{-1} due to the alkyls, there are also many vibrational energies between 1500 and 1700 cm^{-1} favoring to bridge the gap for green emission. Thus, with the decrease of the particle sizes, the green emission is more favored than the red emission, resulting in the high $f_{g/r}$ ratios as observed in ref 23 and our work. Here, the surface effects explain well the opposite behavior of $f_{g/r}$ vs sizes for both the fluoride and oxide UCNPs. To investigate deeper into the surface effects on the $f_{g/r}$ ratios, which were excluded in ref 23 and only the phonon-mediated processes were proposed, the literature's phonon mode (ref 23) was unable to explain the decreasing $f_{g/r}$ ratios with the decrease of the oxide UCNPs. With the reduction of the multiphonon processes in smaller particles populating an energy gap of 5000 cm^{-1} for red emission should decrease more than that of 2000 cm^{-1} for green emission for both the fluoride- and oxide- based UCNPs. Therefore, $f_{g/r}$ should increase in both hosts. Such discussion still needs future studies to confirm. We believe that not only the phonon confinement has to be taken into account in the nanoscale particles but also the surface properties, which could still be dominant in affecting the UC process. Here, the third criterion is then put forward for the instructive study of the UCNPs varying in hosts and surface properties. To compare the UCL of the UCNPs in different hosts (fluorides or oxides), the phonon lattice energy and surface vibrational energies at the NP surface should be considered.

IV. Conclusions

In conclusion, the β-$NaYF_4$:Yb,Er UCNPs in different sizes and shapes are characterized by UC fluorescence spectroscopy, power-dependent UCL, green to red emission ($f_{g/r}$) intensity ratios, and dynamic luminescence decay. The SA/Vol ratios can be applied to compare and explain the UC properties of the prism-shaped UCNPs but not for the differently shaped UCNPs. The shape effect is attributed to the different fractional lattice components in an anisotropic orientational β-nanocrystal in which the *a*-axis and *c*-axis have crystal planes of $\langle 10\bar{1}0\rangle$ and $\langle 0001\rangle$ families, respectively, with different *d*-spacing distances. Therefore, the differently shaped UCNPs could have identical SA/Vol ratios but different lattice energies and therefore different multiphonon relaxation processes in an individual crystal. Aiming at clarifying the current contrast and contradictory observations on the UCL, three general criteria for assessing the UC properties of the UCNPs are proposed. We show that the surface effects are crucial to address many photophysical UC properties, and we believe the observation of the shape effect is of both fundamental and technological interest, suggesting that the photophysical properties of the UCNPs and lanthanide doped NPs can be tailored by changing the particle size as well as the morphology like those widely used in semiconductor quantum dots.

Acknowledgment. This work was supported by the National Science Foundation MRSEC Program through the Princeton Center for Complex Materials (DMR-0819860) and Air Force Office of Scientific Research (AFOSR). We thank Robert H. Austin for the invaluable comments during the paper preparation.

The help from William Ryu, Sanghee Won, Xiaolong Gou, and Wenjun Kong for the dynamic measurement setup is greatly appreciated.

Supporting Information Available: Experimental setup, TEM images, EDS, XRD, and the $f_{g/r}$ ratios of the prism- and rod-shaped UCNPs. This material is available free of charge via the Internet at http://pubs.acs.org.

References and Notes

(1) Chatterjee, D. K.; Rufalhah, A. J.; Zhang, Y. *Biomaterials* **2008**, *29*, 937.
(2) Wang, M.; Mi, C. C.; Wang, W. X.; Liu, C. H.; Wu, Y. F.; Xu, Z. R.; Mao, C. B.; Xu, S. K. *ACS Nano* **2009**, *3*, 1580.
(3) Chatterjee, D. K.; Zhang, Y. *Nanomedicine (London, U.K.)* **2008**, *3*, 73.
(4) Ungun, B.; Prud'homme, R. K.; Budijono, S. J.; Shan, J. N.; Lim, S. F.; Ju, Y. G.; Austin, R. *Opt. Express* **2009**, *17*, 80.
(5) Zhang, P.; Steelant, W.; Kumar, M.; Scholfield, M. *J. Am. Chem. Soc.* **2007**, *129*, 4526.
(6) Kim, W. J.; Nyk, M.; Prasad, P. N. *Nanotechnology* **2009**, *20*, 185301.
(7) Qin, X.; Yokomori, T.; Ju, Y. G. *Appl. Phys. Lett.* **2007**, *90*, 073104.
(8) Kramer, K. W.; Biner, D.; Frei, G.; Gudel, H. U.; Hehlen, M. P.; Luthi, S. R. *Chem. Mater.* **2004**, *16*, 1244.
(9) Suyver, J. F.; Aebischer, A.; Garcia-Revilla, S.; Gerner, P.; Gudel, H. U. *Phys. Rev. B* **2005**, 71.
(10) Suyver, J. F.; Grimm, J.; Kramer, K. W.; Gudel, H. U. *J. Lumin.* **2005**, *114*, 53.
(11) Mai, H. X.; Zhang, Y. W.; Si, R.; Yan, Z. G.; Sun, L. D.; You, L. P.; Yan, C. H. *J. Am. Chem. Soc.* **2006**, *128*, 6426.
(12) Liu, C.; Wang, H.; Li, X.; Chen, D. *J. Mater. Chem.* **2009**, *19*, 3546.
(13) Mai, H. X.; Zhang, Y. W.; Sun, L. D.; Yan, C. R. *J. Phys. Chem. C* **2007**, *111*, 13730.
(14) Qian, H. S.; Zhang, Y. *Langmuir* **2008**, *24*, 12123.
(15) Shan, J.; Ju, Y. *Nanotechnology* **2009**, *20*, 275603.
(16) Shan, J.; Qin, X.; Yao, N.; Ju, Y. *Nanotechnology* **2007**, *18*, 445607.
(17) Shan, J. N.; Ju, Y. G. *Appl. Phys. Lett.* **2007**, *91*, 123103.
(18) Yi, G. S.; Chow, G. M. *Adv. Funct. Mater.* **2006**, *16*, 2324.
(19) Yi, G. S.; Chow, G. M. *Chem. Mater.* **2007**, *19*, 341.
(20) Chen, Z. G.; Chen, H. L.; Hu, H.; Yu, M. X.; Li, F. Y.; Zhang, Q.; Zhou, Z. G.; Yi, T.; Huang, C. H. *J. Am. Chem. Soc.* **2008**, *130*, 3023.
(21) Shan, J. N.; Chen, J. B.; Meng, J.; Collins, J.; Soboyejo, W.; Friedberg, J. S.; Ju, Y. G. *J. Appl. Phys.* **2008**, *104*, 094308.
(22) Mai, H. X.; Zhang, Y. W.; Sun, L. D.; Yan, C. H. *J. Phys. Chem. C* **2007**, *111*, 13721.
(23) Schietinger, S.; Menezes, L. D.; Lauritzen, B.; Benson, O. *Nano Lett.* **2009**, *9*, 2477.
(24) Shan, J.; Yao, N.; Ju, Y. *J. Nanopart. Res.*, in press.
(25) Pollnau, M.; Gamelin, D. R.; Luthi, S. R.; Gudel, H. U.; Hehlen, M. P. *Phys. Rev. B* **2000**, *61*, 3337.
(26) Song, H. W.; Sun, B. J.; Wang, T.; Lu, S. Z.; Yang, L. M.; Chen, B. J.; Wang, X. J.; Kong, X. G. *Solid State Commun.* **2004**, *132*, 409.
(27) Liu, G. K.; Zhuang, H. Z.; Chen, X. Y. *Nano Lett.* **2002**, *2*, 535.
(28) Chen, X. Y.; Zhuang, H. Z.; Liu, G. K.; Li, S.; Niedbala, R. S. *J. Appl. Phys.* **2003**, *94*, 5559.
(29) Li, C. X.; Quan, Z. W.; Yang, J.; Yang, P. P.; Lin, J. *Inorg. Chem.* **2007**, *46*, 6329.
(30) Li, Z. Q.; Zhang, Y. *Nanotechnology* **2008**, 19.
(31) Liang, X.; Wang, X.; Zhuang, J.; Peng, Q.; Li, Y. D. *Adv. Funct. Mater.* **2007**, *17*, 2757.
(32) Sun, Y. J.; Chen, Y.; Tian, L. J.; Yu, Y.; Kong, X. G.; Zhao, J. W.; Zhang, H. *Nanotechnology* **2007**, 18.
(33) Sivakumar, S.; van Veggel, F. C. J. M.; May, P. S. *J. Am. Chem. Soc.* **2007**, *129*, 620.
(34) Yi, G. S.; Chow, G. M. *J. Mater. Chem.* **2005**, *15*, 4460.
(35) Wang, Y.; Tu, L. P.; Zhao, J. W.; Sun, Y. J.; Kong, X. G.; Zhang, H. *J. Phys. Chem. C* **2009**, *113*, 7164.
(36) Busch, G.; Schade, H. *Lect. Solid State Phys.* 1976.
(37) Peng, X. G.; Manna, L.; Yang, W. D.; Wickham, J.; Scher, E.; Kadavanich, A.; Alivisatos, A. P. *Nature* **2000**, *404*, 59.
(38) Empedocles, S. A.; Neuhauser, R.; Bawendi, M. G. *Nature* **1999**, *399*, 126.
(39) Peng, X. G.; Wickham, J.; Alivisatos, A. P. *J. Am. Chem. Soc.* **1998**, *120*, 5343.
(40) De, G. H.; Qin, W. P.; Zhang, J. S.; Zhang, J. H.; Wang, Y.; Cao, C. Y.; Cui, Y. *J. Lumin.* **2006**, *119*, 258.
(41) Heer, S.; Kompe, K.; Gudel, H. U.; Haase, M. *Adv. Mater.* **2004**, *16*, 2102.

JP908976N